Li transport in fresh and aged $LiMn_2O_4$ cathodes via electrochemical strain microscopy

Sergey Yu. Luchkin' , Konstantin Romanyuk, Maxim Ivanov, and Andrei L. Kholkin

Citation: Journal of Applied Physics **118**, 072016 (2015); doi: 10.1063/1.4927816
View online: http://dx.doi.org/10.1063/1.4927816
View Table of Contents: http://aip.scitation.org/toc/jap/118/7
Published by the American Institute of Physics

Li transport in fresh and aged $LiMn_2O_4$ cathodes via electrochemical strain microscopy

Sergey Yu. Luchkin,[1,a)] Konstantin Romanyuk,[1,2] Maxim Ivanov,[1] and Andrei L. Kholkin[1,2]
[1]*Department of Materials and Ceramic Engineering and CICECO, University of Aveiro, 3810 193 Aveiro, Portugal*
[2]*Institute of Natural Sciences, Ural Federal University, 51 Lenin Avenue, 620000 Ekaterinburg, Russia*

(Received 22 December 2014; accepted 10 April 2015; published online 19 August 2015)

Transport properties of Li^+ mobile ions in fresh and aged $LiMn_2O_4$ battery cathodes were studied at the nanoscale via electrochemical strain microscopy (ESM), time spectroscopy, and voltage spectroscopy mapping. Both Vegard and plausible non-Vegard contributions to the ESM signal were identified in electrochemical hysteresis loops obtained on fresh and aged samples. In the fresh cathodes, the Vegard contribution dominates the signal, while in the aged samples different shape of hysteresis loops indicates an additional plausible non-Vegard contribution. Non-uniform spatial distribution of the electrochemical loop opening in $LiMn_2O_4$ particles studied in the aged samples indicates stronger variation of the Li diffusion coefficient at the microscale as compared to the fresh specimens. Time spectroscopy measurements revealed a suppression of the local Li diffusivity in aged samples. The mechanisms of the cathode aging are discussed in the context of observed nanoscale ESM response. © *2015 AIP Publishing LLC*. [http://dx.doi.org/10.1063/1.4927816]

I. INTRODUCTION

Li batteries are of essential importance not only for modern wearable and portable devices but also for growing automotive and green-energy applications. Increasing demand for such applications sets the performance and safety issues still to be solved. Scientific research is currently focusing on creating new battery materials as well as on improving the performance and stability of existing materials. Non-toxic and widely available raw powders of $LiMn_2O_4$ along with their high open-circuit voltage versus Li insertion make them one of the promising cathode materials for Li-ion batteries. However, the possibility of their application in growing fields such as automotive is limited due to poor cycling performance, especially at high C rates. One of the main causes of poor cycling is rapid degradation of $LiMn_2O_4$ active particles. The degradation process occurs via a number of major mechanisms: (i) cracking due to internal stress and loss of electrical contact,[1] (ii) surface degradation due to Mn dissolution caused by the disproportional reaction $2Mn^{3+}_{solid} \rightarrow Mn^{4+}_{solid} + Mn^{2+}_{solution}$,[2] and (iii) structural instability and loss of crystallinity in the bulk due to Li intercalation/deintercalation and associated structural transformations.[3]

A number of modification techniques such as surface coating,[4] doping with suitable elements,[5] and core-shell structuring[6] have been applied to increase the cycling stability of the cathode particles. All these methods could significantly improve the $LiMn_2O_4$ performance. Nevertheless, limited understanding of the degradation mechanisms, especially at high C rates, abridges positive effects of modifications. Therefore, deeper understanding of the degradation of relevant functional properties (e.g., Li ion mobility) at meso- and nano-scales is required.

Conventional electrochemical methods can be hardly used to study Li transport and diffusion at the scale less than several μm. Alternatively, novel method called electrochemical strain microscopy (ESM)[7] is able to probe transport properties of ionically conducting materials at the scale down to a few nm, thus allow better understanding of functionality and degradation mechanisms. Up to now, it has been implemented in multi-frequency band excitation[8] and DART[9] modes on a number of lithium and oxygen conducting materials. The multi-frequency modes make use of resonance amplification without topographic crosstalk associated with the shift of contact resonance frequency during scanning.[10] They are more accurate as compared to the single frequency resonance amplification mode. However, the conventional single frequency mode operating out of the contact resonance (where the frequency response is flat) is not sensitive to the contact resonance frequency shift and thus can be used for ESM imaging.

In this work, we implemented ESM in the single frequency mode[11] to measure the local Li^+ mobility in $LiMn_2O_4$ active particles of the fresh and aged (at 16C-rate) commercial battery cathodes in order to clarify degradation mechanisms at the nanoscale.

II. EXPERIMENTAL

In order to investigate degradation mechanisms of $LiMn_2O_4$ cathodes caused by intensive cycling at high C rate, we compared two commercial 18650 Li-ion battery cells with the graphite anode and the $LiMn_2O_4$ cathode. The first cell ("fresh" sample further in the text) was fully discharged at 1C-rate. The second cell ("aged" sample further in the text) was cycled (106 times) down to 80% State of Health (SOH) at 1C charge rate and 16C discharge rate, then cycled 3 times at 1C-rate and discharged at 1C-rate before opening. The voltage window during cycling was 4.2 2.5 V.

[a)]E mail: luchkin@ua.pt

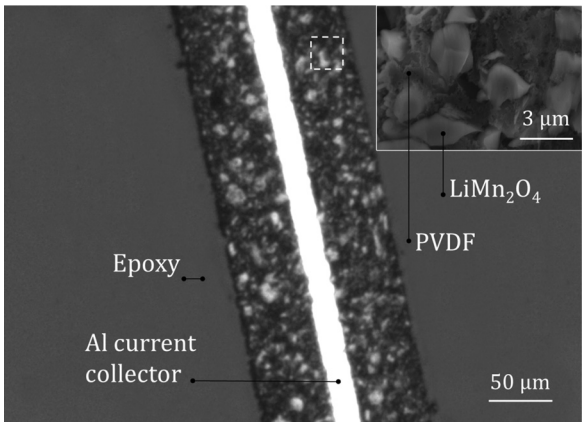

FIG. 1. Optical image of the polished $LiMn_2O_4$ cathode. SEM image of the unpolished cathode is shown in the inset.

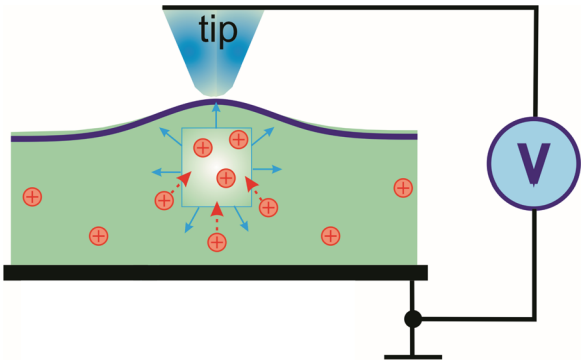

FIG. 2. Schematic illustration of the surface strain caused by the local change of the lattice parameter due to the change of Li concentration under the tip.

After this, $LiMn_2O_4$ cathodes with the Al current collector and PVDF (polyvinylidene fluoride) binder were extracted in a glove box in the Ar atmosphere, washed in dimethyl carbonate (DMC) to remove the electrolyte (solution of $LiPF_6$ in DMC and ethylene carbonate (EC)), embedded in an epoxy resin, and polished mechanically. Final polishing was made by an Ar ion beam. The soft PVDF binder was sputtered off the surface. Cross-section of the polished sample filled by the epoxy is shown in Figure 1.

ESM response was measured using a commercial AFM (Solver Next, NT-MDT) working under ambient conditions. Pt/Ir coated cantilevers with ~5 N/m stiffness and ≈130 kHz resonance frequency were used as external movable electrodes. The samples were grounded through the Al current collector of the cathode serving as a counter electrode. $LiMn_2O_4$ particles are electrically connected to the Al current collector by the PVDF binder enriched with carbon black nanoparticles. Driving ac-voltage of 3 V amplitude and 100 kHz frequency was applied between the sample and the cantilever using the internal source of the microscope. The response was measured by means of the internal lock-in amplifier of the microscope as the first harmonic of the laser beam deflection.

III. ELECTROCHEMICAL STRAIN MICROSCOPY

It is thought that the ESM response in solid mixed electron-ion conductors (MIECs) such as $LiMn_2O_4$ is a result of the Vegard lattice expansion due to small concentration change of mobile Li^+ ions under applied periodic electric field. In general, Li^+ drift velocity consists of field dependent and field independent components and can be expressed as[12]

$$v_i = \frac{D_i}{k_B T}(\nabla\mu_i + z_i F \nabla\varphi), \tag{1}$$

where D_i is the ionic diffusion coefficient, k_B is the Boltzmann constant, T is the temperature, μ_i is the chemical potential, z_i is the ionic charge, F is the Faraday constant, and φ is the electric potential. Redistribution of mobile ions in the applied electric field results in a local molar volume change that leads, in turn, to a local surface strain acquired by the microscope detection system.

According to Ref. 13, the vertical surface displacement (ESM amplitude), proportional to the change of the total number of excess ions (average concentration variation) in the diffuse layer per unit area for the oscillation half-period, can be estimated as

$$u \propto \langle \delta C(t) \rangle \propto \frac{eC_i D_i V_{ac}}{f k_B T R_0}, \tag{2}$$

where e is the elementary charge, C_i is the concentration of mobile ions, D_i is the diffusion coefficient of the mobile ions, V_{ac} is the applied periodic voltage with frequency f, and R_0 is the radius of the tip-sample contact area. A schematic of processes below the tip is shown in Figure 2. Detailed description of the ESM response formation mechanism was given by Morozovska *et al.*[7]

Dynamics of the ESM response reflects instant changes of Li^+ concentration, and therefore, serves as the signature of the Li^+ mobility. It can be measured locally as a function of time by using ESM time spectroscopy.[14] In this technique, a sequence of dc pulses is applied between the tip and the counter electrode, and the surface vibrations (ESM response) are typically measured after the dc pulses. When the dc voltage is on, Li^+ ions migrate under the electric potential gradient $\nabla\phi$ towards or outwards the tip, thus shifting the sample from the initial thermodynamically stable state to a new state with inhomogeneous spatial Li concentration distribution under the field. After the dc bias is off, Li^+ ions diffuse back (relax) bringing the sample from the concentration inhomogeneous state into the initial stable state under the resulting chemical potential gradient $\nabla\mu_i$. Simultaneous ac probing of the ESM response after the dc application represents dynamics of the local strain and presumably Li^+ concentration (this assumption is correct if only C_i changes in Eq. (2)).

Variation of the strain and Li concentration can be also measured as a function of the dc voltage by means of the voltage spectroscopy.[15] In this method, a series of dc pulses (sketched in Figure 3) are applied between the tip and the counter electrode, and the resulting ESM response is probed after each pulse by applying a periodic ac voltage. Measured ESM amplitudes are then plotted versus corresponding dc

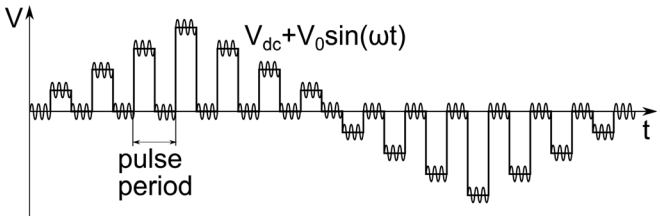

FIG. 3. Schematic representation of the voltage variation during voltage spectroscopy measurements in ESM.

voltages. As the field induced Li^+ concentration increases/decreases below the tip, the strain correspondingly increases/decreases according to Eq. (2). Short time between pulses prevents full strain relaxation after each pulse, thus electrochemical hysteresis loops can be observed, resembling the conventional piezoresponse hysteresis loops in ferroelectric materials.[16] In contrast to ferroelectrics where hysteresis is a signature of polarization switching, ESM loops rather represent a variation of Li^+ concentration/mobility that follows dc voltage cycling.

It has been previously shown[15] that the ESM loop's shape is controlled by the relaxation kinetics and thermodynamics of the electrochemical reaction. The representative results are shown in Figure 4. Here, we measured electrochemical loops for three different times after dc pulses on the fresh sample at the same location. The obtained loops' shapes are similar to those reported by Balke *et al.*[17]

IV. NON-VEGARD CONTRIBUTIONS

In addition to the Vegard ESM response u, a number of other non-Vegard contributions to the measured signal $A_{1\omega}$ are possible[18]

$$A_{1\omega} \propto -\frac{(1+\nu)}{\pi}h\left(\left(\beta-\frac{2q}{\varepsilon\varepsilon_0}f_{33}\right)\langle\delta C(t)\rangle+\Xi_{33}^{C}\langle\delta n(t)\rangle+\Xi_{33}^{V}\langle\delta p(t)\rangle+\frac{\tilde{Q}_{33}k_BT}{2\varepsilon\varepsilon_0}\langle E_3^2\rangle\right)+\frac{1}{k}\frac{\partial C}{\partial z}(V_{dc}+V_C)V_{ac}+d_{33}V_{ac}, \quad (3)$$

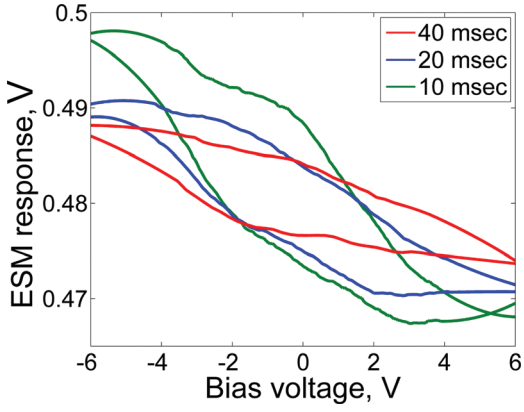

FIG. 4. Voltage spectroscopy (electrochemical hysteresis loops) measured for 10, 20, and 40 ms pulse durations.

where ν is the Poisson coefficient, h is the film thickness (in case of a thin film sample), $\left(\beta-\frac{2q}{\varepsilon\varepsilon_0}f_{33}\right)$ is the renormalized Vegard coefficient including flexoelectric strain tensor components f_{33}, Ξ_{33}^{C}, and Ξ_{33}^{V} are the deformation potential tensors for electron and hole contributions correspondingly, $\tilde{Q}_{33}$ is the electrostriction coefficient, $E_3=-\frac{\partial\varphi(z)}{\partial z}$ is the electric field distribution, $\frac{1}{k}\frac{\partial C}{\partial z}(V_{DC}-V_C)V_{AC}$ is the electrostatic contribution,[16] and $d_{33}^{eff}V_{AC}$ is the piezoresponse.[16] $\langle\delta C(t)\rangle$, $\langle\delta n(t)\rangle$, and $\langle\delta p(t)\rangle$ are the concentration variations of ions, electrons, and holes as functions of the applied voltage V_{ac} (for example, $\langle\delta C(t)\rangle\propto\frac{eC_iD_iV_{ac}}{fk_BTR_0}$).

For $Li_xMn_2O_4$, the lattice parameter changes almost linearly from 8.03 Å for λ-MnO_2 to 8.24 Å for $LiMn_2O_4$. Taking into account that the dynamic resolution of ESM is about 10 pm (using a lock-in amplifier), we can detect about 5% of Li concentration variation in the unit cell (on average).

Flexoelectric and deformation potential contributions for $LiMn_2O_4$ are not known, but typically they are an order of magnitude smaller than the Vegard contribution.[18]

Electrostatic contribution due to the contact potential difference between the tip and the sample does not change the hysteresis loop shape measured in the off-field state.[16] It just shifts the whole loop along the ESM response axis causing an offset which depends on the tip electrode material. However, this is not always true. Sufficiently high voltage applied to the tip in a contact with the sample can cause charge injection. Typical space charge relaxation time (also known as Maxwell-Wagner relaxation time) for $LiMn_2O_4$ with the static dielectric permittivity ≈10 (Ref. 19) and electrical conductivity $\sim10^{-6}$ S/cm (Ref. 12) does not exceed $\sim10^{-6}$s. Nevertheless, if charge traps are present, the space charge state can be stabilized and its relaxation time can significantly exceed 10^{-6}s. If the relaxation is longer than the probing time after the dc voltage pulse application, space charge can also contribute to an off-field signal. This phenomenon has been demonstrated in perovskite manganite $La_{0.89}Sr_{0.11}MnO_3$.[20]

The response is not limited by the above mentioned general contributions. Under these circumstances, specific properties of $Li_xMn_2O_4$ have to be considered in order to evaluate possible non-Vegard contributions. This step is essential for correct interpretation of results.

$LiMn_2O_4$ is a small polaron semiconductor[21] with centrosymmetric Fd3m cubic crystal structure (centrosymmetric structure rules out piezoelectric effect). It undergoes cubic Fd3m to orthorhombic Fddd phase transformation around room temperature (~280 300 K) upon cooling/heating.[22] Another phase transformation from cubic Fd3m to tetragonal I41/amd crystal structure occurs during Li intercalation when x exceeds 1 in $Li_xMn_2O_4$ (average Mn^{n+} oxidation state ≤3.5).[23] Conventional Li diffusion mechanism suggests that Li^+ ions simply hop over vacant 8a and 16c positions in the crystal lattice.[24] However, the small polaron hopping mechanism of electrical conductivity is not consistent with it.[22,24] Therefore, Tateishi *et al.*[25] suggested another mechanism of Li diffusion, where hopping of Mn^{3+} e_g electron mediates O^{2-} ion displacement and allows Li to pass from

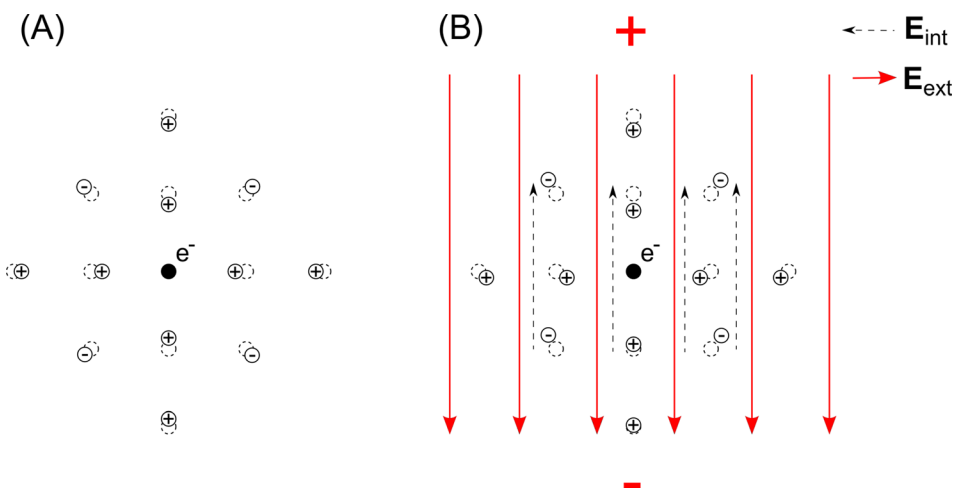

FIG. 5. (a) Schematic representation of a polaron and (b) dipole moment induced in the polaron by the external electric field.

one position to another. This supposition is in agreement with the anti-adiabatic limit for small polarons, where ions adiabatically follow the motion of electrons.[26]

Following this approach, the external electric field applied in the ESM experiment between the tip and the counter electrode should induce a dipole moment of the small polarons[27] (as schematically shown in Figure 5) and their ordering along with the true ionic ESM response. This contribution can be more complex in the case when local Li/Mn ratio below the tip can exceed the first order Jahn-Teller distortion threshold (average Mn^{n+} oxidation state ≤ 3.5) and induce the lattice transformation.[23] Though the first order Jahn-Teller distortion does not break the inversion symmetry, the structural transformation/electrochemical reaction can manifest itself as butterfly-like amplitude response and phase switching that were observed under very high applied voltage.[28] Additionally, static long-range ordering of Jahn-Teller polarons and local charge ordering under external electric field in manganites can induce lattice distortion that can break the structural inversion symmetry and provoke local ferroelectric-like response.[20,29–31] Though it was not reported in $LiMn_2O_4$ so far, we cannot exclude a possibility of emergence of ferroelectric-like state (localized in time and space), which is difficult to assess numerically.

Ferroelectric and dipole non-Vegard contributions considered above are polar and should have the characteristic butterfly-like shape of the amplitude hysteresis loop and 180° phase switching, while the ESM amplitude loop has different shapes and its phase does not switch at 180° due to non-polar nature of the Vegard strain response,[32] which depends only on Li concentration (see Eq. (2)). In our case, the measured ESM loops do not have the distinct butterfly-like shape and phase switching, which means that above mentioned non-Vegard mechanisms do not contribute significantly to the ESM response. However, in the aged sample, the shape of the loops noticeably differs from those taken on

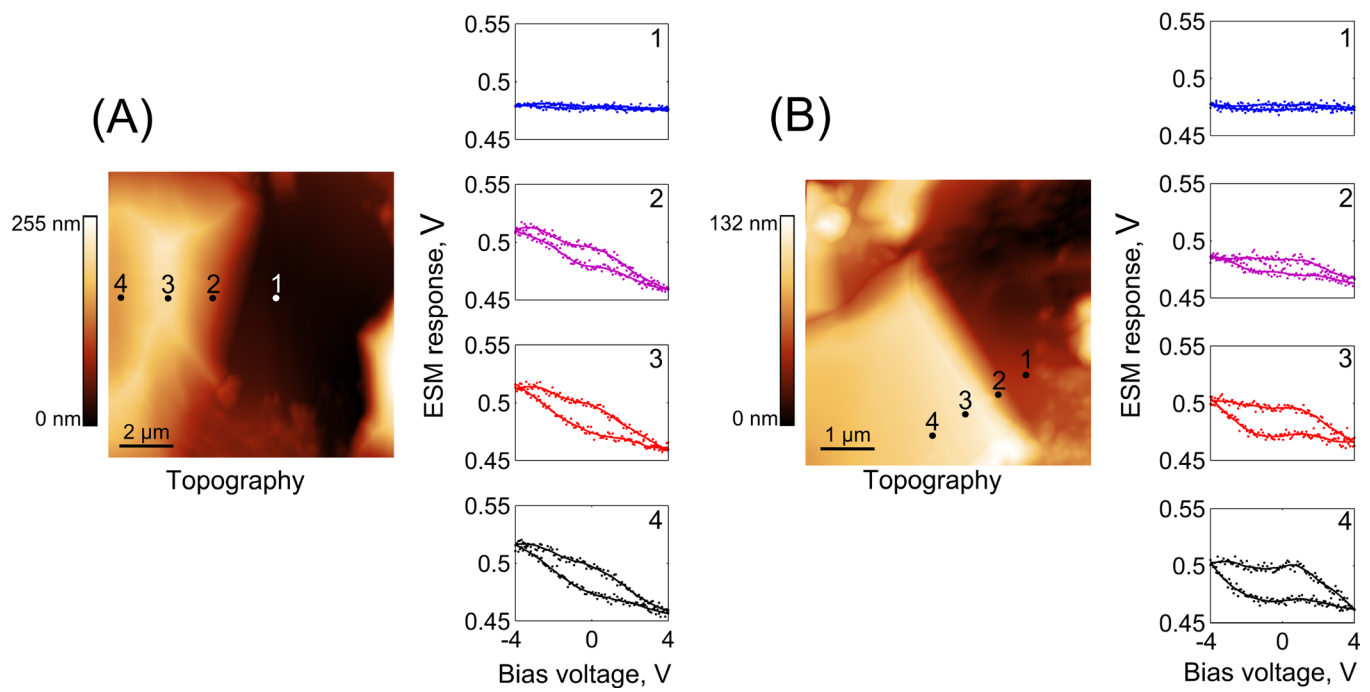

FIG. 6. (a) ESM loops on the fresh cathode and (b) ESM loops on the aged cathode. Each loop is an average of 3 loops measured consequently at the same point. Reprinted with permission from Romanyuk *et al.*, Microsc. Microanal. **21**, 154 163 (2015). Copyright 2015 Cambridge University Press.

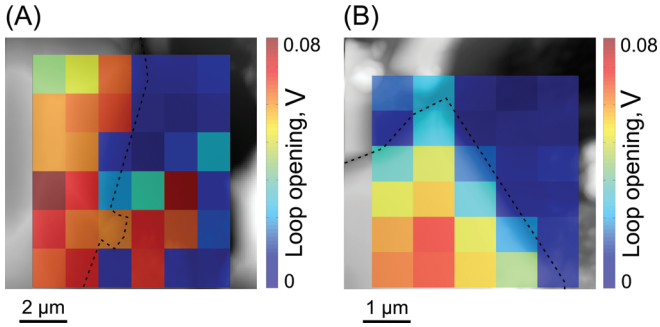

FIG. 7. Mapping of loop opening on fresh (a) and aged (b) samples. Dashed line traces the particles edges.

the fresh sample. This could be attributed to a stronger contribution of the non-Vegard terms (discussed in detail below).

V. RESULTS AND DISCUSSION

Preliminary X-Ray Diffraction (XRD) and Inductively coupled plasma optical emission spectrometry (ICP-OES) measurements showed that the fresh sample possesses spinel Fd3m cubic structure with lattice parameter of 8.1779 Å and Li:Mn ratio of 0.94:2; the aged sample has the same spinel Fd3m cubic structure with lattice parameter of 8.1791 Å and Li:Mn ratio of 0.89:2. It should be noted that ICP-OES cannot distinguish the origin of different elements. It is hence possible that lithium was present as an impurity (secondary electrolyte interface, rest of electrolyte salts, etc.), thus increasing the overall ratio.

Figure 6 compares the electrochemical hysteresis loops measured on the (a) fresh and (b) aged samples. Loops 1 on both samples were obtained from the epoxy that filled porosity in the binder. They are expectedly closed because there are no mobile ions responsible for the ESM response. Loops 2, 3, and 4 were obtained on different places within $LiMn_2O_4$ particles. They are open, clearly indicating the presence of mobile Li^+ ions. The ESM hysteresis loops from the fresh sample are uniformly open over the particle with the response gradually changing with the applied dc voltage (corresponding to change of Li^+ concentration and strain below the tip according to Eq. (2)). In contrast, stronger variation of the loop opening was observed on the aged sample. As compared to the loops from the fresh sample, they have noticeably different shapes with characteristic plateaus on top and bottom that bend with wider loop opening.

Considering only the Vegard contribution, such increase of the loop opening can be explained by lower Li^+ diffusion coefficient. Taking into account a complex dependence of the Li diffusion coefficient on Li concentration,[33] the observed change of the loop's shape can indicate also a wider variation of the Li diffusion coefficient over the dc voltage cycle in the aged sample.

Alternatively, change of the loop's shape can indicate an additional non-Vegard contribution.[34] The ratio of the Vegard (ionic) to the non-Vegard contributions can control the final shape of the hysteresis loop. In view of the complex nature and multiple sources of the total non-Vegard contribution, it is hard to estimate it numerically.

Electrochemical hysteresis loops measured over a grid of points on an active particle surface can reveal distribution of electrochemical activity, e.g., Li^+ mobility/concentration as a function of the position. Figure 7 shows topography images of the (a) fresh and (b) aged samples overlaid with the electrochemical loop opening map. On the epoxy, the loops are closed as expected. On the active particles, the loops are open. Loop opening is relatively uniform for the fresh sample. In contrast, loop opening in the aged sample is less uniform, sometimes with gradient towards the particle center.

Further insight into functionality and degradation of $LiMn_2O_4$ can be done by using the time spectroscopy. Here, we measured ESM response not only when dc voltage is off but also when dc voltage is on to observe both the migration and diffusion processes.[35] Figure 8 illustrates the time spectroscopy measurements on both fresh and aged samples taken on $LiMn_2O_4$ particles. Figure 9 displays the migration/relaxation processes on the aged sample at different points on the particle surface.

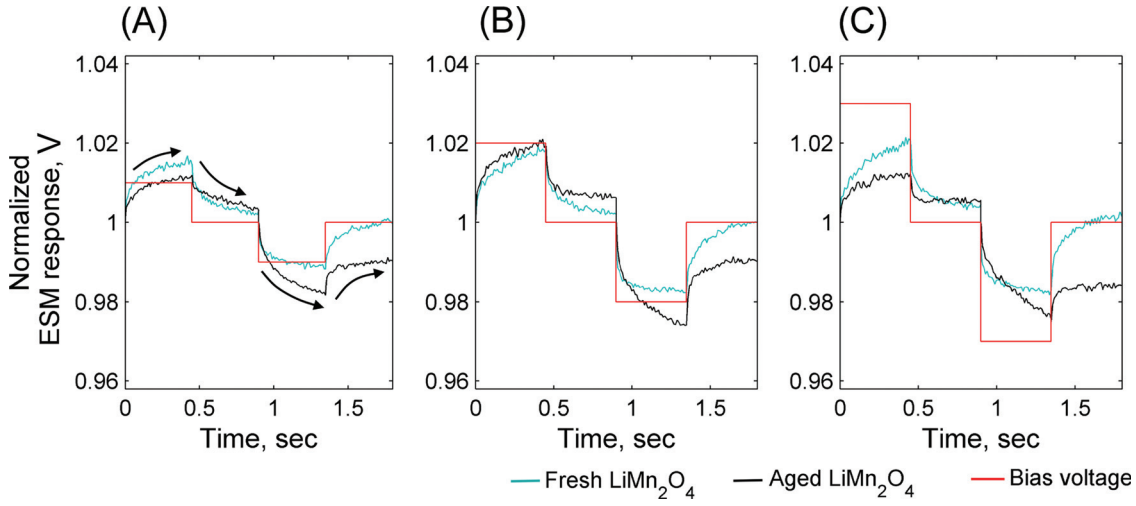

FIG. 8. Time dependence of the ESM response. 500 ms dc voltage pulses of ±3 (a), ±4 (b), and ±5 V (c) were applied red line. ESM response during and after the pulses is measured as a function of time on the fresh (blue line) and aged (black line) samples. Curves were averaged over 10 consequent measure ments from a single point. Electrostatic linear contribution (when the dc is on) was subtracted.[34]

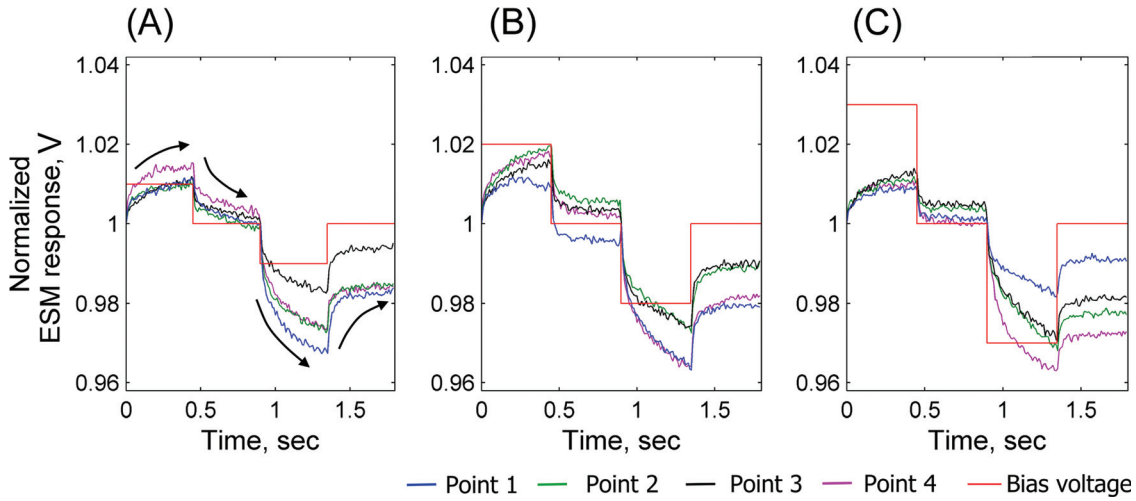

FIG. 9. Different points from the aged $LiMn_2O_4$ particles. 500 ms dc voltage pulses of ±3 (a), ±4 (b), and ±5 V (c) were applied red line. ESM response during and after the pulses is measured as a function of time. Each curve was averaged over 10 consequent measurements from a single point. Electrostatic lin ear contribution (when the dc bias is on) was subtracted.[34]

ESM response increases during application of the dc pulse on the fresh sample, i.e., when migration of Li^+ ions is induced by the electric field. When dc bias is off, the ESM response relaxes reflecting Li diffusion to the initial state. For the aged sample, the migration in the electric field is stronger than the following relaxation, and it is not symmetrical with respect to 0 V. The relaxation process is therefore not complete.

Following Jesse *et al.*,[35] we estimated the characteristic diffusion times for volumes typically probed by ESM in $LiMn_2O_4$. For the probed diffusion length equal to the tip radius $R_0 \approx 30$ nm and $D_{Li} = 10^{-12}$ 10^{-10} cm^2 s^{-1} (Ref. 33), the characteristic diffusion time $\tau = \frac{l^2}{D} = 0.1$ 10 s. In order to compare the diffusion coefficients of Li in the fresh and aged samples, we fitted the relaxation (dc bias off) curves from Figure 8 by using exponential function

$$u(o,t) = u_0 + A_1 \exp\left(-\frac{t-t_0}{\tau_1}\right) + A_2 \exp\left(-\frac{t-t_0}{\tau_2}\right).$$

Characteristic decay times $\tau_1 \sim 10^{-3}$ s and $\tau_2 \sim 0.1$ 10 s were extracted.[34] The slow decay time $\tau_2 \sim 0.1$ 10 s is in agreement with the estimated diffusion time and was used to estimate the Li diffusion coefficients via equation $D = \frac{l^2}{\tau}$. The diffusion coefficients are plotted in Figure 10 as a function of the applied voltage.

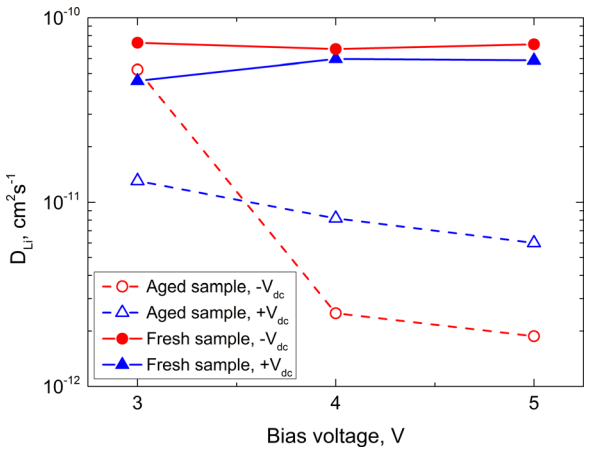

FIG. 10. Li diffusion coefficients as a function of dc bias calculated for the relaxation curves of Figure 8 for the fresh and aged $LiMn_2O_4$.

The estimated $D_{Li} \sim 10^{-10}$ cm^2 s from the fresh sample is stable vs bias voltage and slightly lower after the positive dc pulses as compared to the negative ones. The diffusion coefficients from the aged sample are 1 2 orders of magnitude lower and decrease with the bias voltage, especially after the negative bias, where D_{Li} drops by 2 orders of magnitude.

Decrease of the Li diffusion coefficient observed on the polished cross-sections of the $LiMn_2O_4$ particles can be attributed to two reasons: (i) decrease of the local structural order due to increased concentration of point defects and (ii) cubic to tetragonal phase transition.

(i) Increased concentration of point defects (vacancies, interstitials, and composition change of Mn and O atoms) induced by cyclic Li insertion and extraction[36] is a common cause of the Li diffusion reduction because it leads to a partial destruction of the Li transport network within the spinel host structure.

(ii) The tetragonal phase of the lithium manganese oxide has the Li diffusion coefficient that is about an order of magnitude lower than the cubic one.[37] Transition from cubic to tetragonal phase below the tip can happen due to local overpotential, thus decreasing the diffusion coefficient. Nucleation of a new phase occurs predominantly inhomogeneously on defects, in which the nucleation barrier ΔG is smaller. Thus, a sample with higher concentration of defects under the same conditions is expected to experience earlier phase transition and apparent reduction of the diffusion coefficient.

The comparison of discussed above mechanisms suggest that the diffusion coefficient reduction in the aged $LiMn_2O_4$ sample is because of higher concentration of point defects. Indeed, the data were obtained on the polished cross-section of the particles and cannot be attributed to the surface Mn dissolution caused by the disproportional reaction

$2Mn^{3+}_{solid} \rightarrow Mn^{4+}_{solid} + Mn^{2+}_{solution}$ or other surface degradation effects, whereas Li insertion/extraction and associated effects (such as instability of delithiated spinel and onset of the Jahn-Teller distortion in the lithiated spinel) affect the whole particle, increasing concentration of point defects. This mechanism is especially important in the case of 16C-rate of discharge, when local Li concentration in a $LiMn_2O_4$ particle can exceed the cubic to tetragonal transformation threshold.[38]

Unsaturated and asymmetric electromigration parts of the time spectroscopy data (shown in Figure 9) as well as the characteristic plunge in the beginning of the relaxation curves could indicate additional non-Vegard contributions as discussed above. It is worth to point out that such effects have to be considered in order to prevent possible misinterpretation of experimental results, especially in complex oxides. Moreover, they could serve as sources of additional information about the materials properties.

Previously reported drop of Li diffusion coefficient during ageing was attributed to the Mn dissolution and increase of surface resistivity.[39] Our results suggest that it is not the only reason of Li diffusion reduction and the structural instability at high C-rates could extensively contribute to $LiMn_2O_4$ degradation as compared to low and moderate C-rates. Additional information can be obtained by macroscopic measurements of Li diffusion coefficient at different C-rates and SOH in bare $LiMn_2O_4$ particles and the ones with coating reducing Mn dissolution.[4]

VI. CONCLUSION

In conclusion, we have measured the ESM response on the fresh and aged $LiMn_2O_4$ cathodes of commercial Li-batteries. Voltage spectroscopy showed less uniform distribution of loop opening on the aged $LiMn_2O_4$ particles as compared to the fresh ones. Time spectroscopy revealed a reduction of Li diffusivity in the aged $LiMn_2O_4$. The local diffusion coefficients were numerically estimated and demonstrated a decrease of the diffusion coefficient in the aged samples by 1 2 orders of magnitude as compared to the fresh ones. These effects were attributed to the structural degradation during 16C-rate cycling. Mechanisms of the non-Vegard contributions to the ESM response were discussed.

ACKNOWLEDGMENTS

The work was supported by the European Commission within FP7 Marie Curie Initial Training Network "Nanomotion" (Grant Agreement No. 290158). K. Romanyuk is grateful to the financial support of FCT via his postdoctoral Grant No. SFRH/BPD/88362/2012. The authors gratefully acknowledge H.-Y. Amanieu and D. Rosato (Robert Bosch GmbH) for providing cathode samples and valuable discussions. XRD and ICP-OES measurements were made by Robert Bosch GmbH. The equipment of the Ural Center for Shared Use "Modern nanotechnology" UrFU was used. The research was made possible, in part, by the Ministry of Education and Science of the Russian Federation (Agreement 14.594.21.0011, ID RFMEFI59414X0011). The authors acknowledge the support of CICECO and FCT via a Grant No. Pest-C/CTM/LA0011/013.

[1]W. H. Woodford, Y. M. Chiang, and W. C. Carter, J. Electrochem. Soc. **157**, A1052 (2010).
[2]D. H. Jang, J. Electrochem. Soc. **143**, 2204 (1996).
[3]H. Xia, Z. Luo, and J. Xie, Prog. Nat. Sci.: Mater. Int. **22**, 572 (2012).
[4]X. Wu, R. Li, S. Chen, and Z. He, Rare Met. **28**, 122 (2009).
[5]B. Deng, H. Nakamura, Q. Zhang, M. Yoshio, and Y. Xia, Electrochim. Acta **49**, 1823 (2004).
[6]J. Tu, X. B. Zhao, J. Xie, G. S. Cao, D. G. Zhuang, T. J. Zhu, and J. P. Tu, J. Alloys Compd. **432**, 313 (2007).
[7]A. N. Morozovska, E. A. Eliseev, N. Balke, and S. V. Kalinin, J. Appl. Phys. **108**, 053712 (2010).
[8]S. Jesse, S. V. Kalinin, R. Proksch, A. P. Baddorf, and B. J. Rodriguez, Nanotechnology **18**, 435503 (2007).
[9]B. J. Rodriguez, C. Callahan, S. V. Kalinin, and R. Proksch, Nanotechnology **18**, 475504 (2007).
[10]S. Jesse and S. V. Kalinin, J. Phys. D: Appl. Phys. **44**, 464006 (2011).
[11]K. Romanyuk, S. Y. Luchkin, M. Ivanov, A. Kalinin, and A. L. Kholkin, Microsc. Microanal. **21**, 154 163 (2015).
[12]M. Park, X. Zhang, M. Chung, G. B. Less, and A. M. Sastry, J. Power Sources **195**, 7904 (2010).
[13]A. Tselev, A. N. Morozovska, A. Udod, E. A. Eliseev, and S. V. Kalinin, Nanotechnology **25**, 445701 (2014).
[14]S. Guo, S. Jesse, S. Kalnaus, N. Balke, C. Daniel, and S. V. Kalinin, J. Electrochem. Soc. **158**, A982 (2011).
[15]A. Kumar, F. Ciucci, A. N. Morozovska, S. V. Kalinin, and S. Jesse, Nat. Chem. **3**, 707 (2011).
[16]S. Hong, J. Woo, H. Shin, J. U. Jeon, Y. E. Pak, E. L. Colla, N. Setter, E. Kim, and K. No, J. Appl. Phys. **89**, 1377 (2001).
[17]N. Balke, S. Jesse, Y. Kim, L. Adamczyk, A. Tselev, I. N. Ivanov, N. J. Dudney, and S. V. Kalinin, Nano Lett. **10**, 3420 (2010).
[18]S. V. Kalinin and A. N. Morozovska, J. Electroceram. **32**, 51 (2014).
[19]K. Hoang, J. Mater. Chem. A **2**, 18271 (2014).
[20]R. F. Mamin, I. K. Bdikin, and A. L. Kholkin, Appl. Phys. Lett. **94**, 222901 (2009).
[21]E. Iguchi, Y. Tokuda, H. Nakatsugawa, and F. Munakata, J. Appl. Phys. **91**, 2149 (2002).
[22]J. Molenda, Solid State Ionics **175**, 203 (2004).
[23]H. Berg, K. Goransson, B. Nolang, and J. O. Thomas, J. Mater. Chem. **9**, 2813 (1999).
[24]N. Ishizawa and K. Tateishi, J. Ceram. Soc. Jpn. **117**, 6 (2009).
[25]K. Tateishi, D. du Boulay, and N. Ishizawa, Appl. Phys. Lett. **84**, 529 (2004).
[26]J. T. Devreese, *Encyclopedia of Applied Physics* (Wiley, 2003), p. 383.
[27]Y. A. Firsov, *Polarons* (Nauka, Moscow, 1975), p. 424.
[28]J. S. Sekhon, L. Aggarwal, and G. Sheet, Appl. Phys. Lett. **104**, 162908 (2014).
[29]Q. Li, Y. Liu, D. Wang, R. L. Withers, Z. Li, H. Luo, and Z. Xu, Appl. Phys. Lett. **101**, 242906 (2012).
[30]C. Jooss, L. Wu, T. Beetz, R. F. Klie, M. Beleggia, M. A. Schofield, S. Schramm, J. Hoffmann, and Y. Zhu, Proc. Natl. Acad. Sci. U. S. A. **104**, 13597 (2007).
[31]F. G. N. Figueiras, I. K. Bdikin, V. B. S. Amaral, and A. L. Kholkin, Phys. Chem. Chem. Phys. **16**, 4977 (2014).
[32]Q. N. Chen, Y. Ou, F. Ma, and J. Li, Appl. Phys. Lett. **104**, 242907 (2014).
[33]M. D. Chung, J. H. Seo, X. C. Zhang, and A. M. Sastry, J. Electrochem. Soc. **158**, A371 (2011).
[34]See supplementary material at http://dx.doi.org/10.1063/1.4927816. Figure S1 shows Vegard and non Vegard hysteresis loops. Figure S2 shows the subtracted electrostatic response. Figure S3 shows additional voltage spec troscopy loops. Figure S4 shows estimated diffusion times.
[35]S. Jesse, N. Balke, E. Eliseev, A. Tselev, N. J. Dudney, A. N. Morozovska, and S. V. Kalinin, ACS Nano **5**, 9682 (2011).
[36]K. Kanamura, H. Naito, T. Yao, and Z. Takehara, J. Mater. Chem. **6**, 33 (1996).
[37]J. Barker, R. Pynenburg, and R. Koksbang, J. Power Sources **52**, 185 (1994).
[38]K. Y. Chung and K. B. Kim, Electrochim. Acta **49**, 3327 (2004).
[39]S. R. Das, S. B. Majumder, and R. S. Katiyar, J. Power Sources **139**, 261 (2005).